RSC Advances

ROYAL SOCIETY OF CHEMISTRY

www.rsc.org/advances

Graphical Abstract

By introduction of 4,4'-bipyridine (4,4′-bipy) as a second organic ligand, two new nickel(II) carboxyphosphonates with a 3D framework structure, namely, $[Ni_3(H_2L)_2(4,4'\text{-bipy})(H_2O)_4]$ (**1**) and $[Ni_3(H_2L')_2(4,4'\text{-bipy})_2(H_2O)_2]\cdot 4H_2O$ (**2**) (H_5L = 4-{[bis(phosphonomethyl)amino]methyl}benzoic acid; H_5L' = *N,N*-bis(phosphonomethyl)aminoacetic acid) have been synthesized under hydrothermal conditions. Compounds **1** and **2** both feature three-dimensional (3D) framework structures with two-dimensional (2D) layers pillared by 4,4′-bipy. For compound **1**, $\{Ni(1)O_4N_2\}$, $\{Ni(2)O_6\}$ and $\{CPO_3\}$ polyhedra form a 2D inorganic player in the *bc*-plane *via* corner-sharing. Then adjacent layers are further pillared by 4,4′-bipy ligands into a 3D pillar-layered structure. In compound **2**, $\{Ni(1)O_4N_2\}$, $\{Ni(2)O_4N_2\}$ and $\{CPO_3\}$ polyhedra are interconnected by carboxyphosphonate ligands to a 2D layer in the *ab*-plane. Neighboring layers are further cross-linked *via* 4,4'-bipy ligands, generating a 3D framework structure. Whereas the carboxylate oxygen atoms of carboxyphosphonate ligands are coordinated to Ni(II) atoms in compound **2** but not in compound **1**. The surface photovoltage and luminescent properties of compounds **1** and **2** have been investigated at the same time.

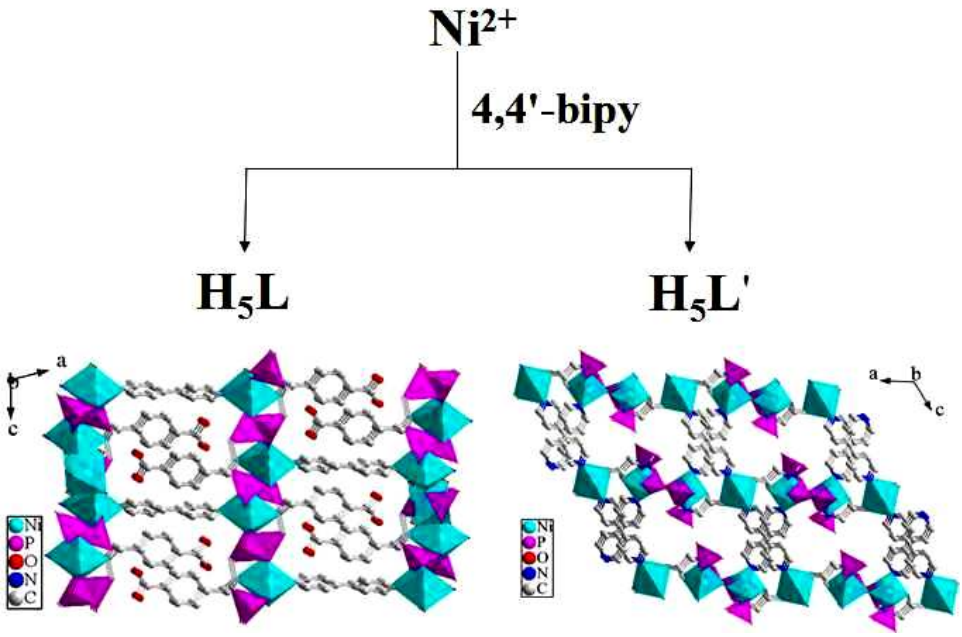

Synthesis, structures, surface photovoltage and luminescent properties of two new nickel(II) carboxyphosphonates with a 3D framework structure

Hui Luo, Yan-Yu Zhu, Zhen-Gang Sun,* Cheng-Qi Jiao, Guang-Ning Zhang, Tong Sun, Ming-Xue Ma and Wen-Zhu Li

School of Chemistry and Chemical Engineering, Liaoning Normal University, Dalian 116029, P. R. China

By introduction of 4,4'-bipyridine (4,4′-bipy) as a second organic ligand, two new nickel(II) carboxyphosphonates with a 3D framework structure, namely, $[Ni_3(H_2L)_2(4,4'\text{-bipy})(H_2O)_4]$ (**1**) and $[Ni_3(H_2L')_2(4,4'\text{-bipy})_2(H_2O)_2]\cdot 4H_2O$ (**2**) (H_5L = 4–{[bis(phosphonomethyl)amino]methyl}benzoic acid; H_5L' = *N,N*–bis(phosphonomethyl)aminoacetic acid) have been synthesized under hydrothermal conditions. Compounds **1** and **2** both feature three-dimensional (3D) framework structures with two-dimensional (2D) layers pillared by 4,4′-bipy. For compound **1**, $\{Ni(1)O_4N_2\}$, $\{Ni(2)O_6\}$ and $\{CPO_3\}$ polyhedra form a 2D inorganic player in the *bc*-plane *via* corner-sharing. Then adjacent layers are further pillared by 4,4′-bipy ligands into a 3D pillar-layered structure. In compound **2**, $\{Ni(1)O_4N_2\}$, $\{Ni(2)O_4N_2\}$ and $\{CPO_3\}$ polyhedra are interconnected by carboxyphosphonate ligands to a 2D layer in the *ab*-plane. Neighboring layers are further cross-linked *via* 4,4'-bipy ligands, generating a 3D framework structure. Whereas the carboxylate oxygen atoms of carboxyphosphonate ligands are coordinated to Ni(II) atoms in compound **2** but not in compound **1**. The surface photovoltage and luminescent properties of compounds **1** and **2** have been investigated at the same time.

Introduction

The chemistry of the metal phosphonates has been a research field of rapid expansion in recent decades, mainly due to their structure diversities and potential applications in catalysis, ion exchange, magnetism, proton conductivity, photochemistry, molecular recognition and materials chemistry.[1]

* To whom correspondence should be addressed: E–mail: szg188@163.com

Therefore, the rational design and synthesis of novel metal phosphonates with the intriguing diversity of architectures and properties has become a particularly important subject. In order to achieve this aim, the strategy of attaching functional groups such as carboxylic acids, crown ethers and amines to the phosphonic acid has been proved to be an effective method, since it can provide various kinds of coordination modes under different reaction conditions which may result in novel structures and interesting properties.[2] During the past few years, a series of metal phosphonates with functionalized phosphonic acids have been isolated in our laboratory.[3] Another important and useful strategy of building new types of metal phosphonates has been concerned with the synthesis of hybrid frameworks by incorporating a second organic ligand such as carboxylic acid, oxalate, sulfonic acids, 2,2'-bipyridine, 4,4'-bipyridine, or 1,10-phenanthroline into the structures of metal phosphonates.[4] Recently, a series of novel metal phosphonate hybrids with mixed ligands have also been obtained by our group.[5] Results from ours and other groups indicate that the introduction of a second organic ligand has been found to be an effective synthetic method in the synthesis of metal phosphonates with new structure types and interesting properties, since these molecules can act as pillars between neighboring layers or be grafted into the inorganic layer to form new hybrid architectures. In the present paper, by employing 4–{[bis(phosphonomethyl)amino]methyl}benzoic acid (H_5L) or *N,N*–bis(phosphonomethyl)aminoacetic acid (H_5L') as the phosphonate ligand and 4,4'-bipy as the second metal linker, we have successfully obtained two new nickel(II) carboxyphosphonates with a 3D framework structure, namely, $[Ni_3(H_2L)_2(4,4'\text{-bipy})(H_2O)_4]$ (**1**) and $[Ni_3(H_2L')_2(4,4'\text{-bipy})_2(H_2O)_2]\cdot 4H_2O$ (**2**). To our knowledge, research on the properties of metal phosphonates is mainly focused on the magnetism, luminescence, proton conductivity and ion exchange etc, there are few reports about photoelectric property of these materials. Surface photovoltage spectroscopy (SPS) is an effective tool to investigate the charge change of the solid surface, which can be used to survey the photophysics of the excited states and the surface charge behavior of the sample.[6] The reports on this aspect are mainly involved in the coordination complexes with phthalocyanines, porphyrins or carboxylic acid as ligands.[7] Recently, only a few investigations on the surface photovoltage property of metal phosphonates have been reported by our group.[8] Herein we report the syntheses, crystal structures, surface photovoltage and luminescent properties of two title compounds.

Experimental

Materials and measurements

The 4–{[bis(phosphonomethyl)amino]methyl}benzoic acid (H_5L) and *N,N*–bis(phosphonomethyl)aminoacetic acid (H_5L') were synthesized according to procedures described previously.[9] All other chemicals were obtained from commercial sources and used without further purification. C, H and N content were determined by using a PE–2400 elemental analyzer. Ni and P content were determined by using an inductively coupled plasma (ICP) atomic absorption spectrometer. IR spectra were recorded on a Bruker AXS TENSOR–27 FT–IR spectrometer with KBr pellets in the range 4000–400 cm^{-1}. The X-ray powder diffraction data was collected on a Bruker AXS D8 Advance diffractometer using Cu–Kα radiation (λ = 1.5418 Å) in the 2θ range of 5–60° with a step size of 0.02° and a scanning rate of 3°/min. TG analyses were performed on a Perkin–Elmer Pyris Diamond TG thermal analyses system in static air with a heating rate of 10 K min^{-1} from 50 °C to 1100 °C. Surface photovoltage spectroscopy (SPS) and field–induced surface photovoltage spectroscopy (FISPS) measurements were conducted with the sample in a sandwich cell (ITO/sample/ITO) with the light source-monochromator-lock-in detection technique. The luminescence spectra were reported on a HITACHI F–7000 spectrofluorimeter (solid).

Synthesis of $[Ni_3(H_2L)_2(4,4'\text{-bipy})(H_2O)_4]$ (1). A mixture of $NiCl_2{\cdot}6H_2O$ (0.24 g, 1 mmol), H_5L (0.17 g, 0.5 mmol) and 4,4'-bipy (0.09 g, 0.5 mmol) was dissolved in 10 mL distilled water, and then stirred for about 1 hour at room temperature. The mixture (pH = 6.0) was sealed in a 20 mL Teflon–lined stainless steel autoclave and heated at 170 °C for 5 days under autogenous pressure. After the mixture was cooled slowly to room temperature, the green block crystals of **1** were obtained. Yield 44.6 % (based on Ni). Anal. Calc. for $C_{30}H_{40}N_4O_{20}P_4Ni_3$: C, 33.50; H, 3.75; N, 5.20; P, 11.51; Ni, 16.32. Found: C, 33.46; H, 3.78; N, 5.23; P, 11.46; Ni, 16.38 %. IR (KBr, cm^{-1}): 3582(m), 3523(m), 1702(m), 1650(m), 1612(s), 1540(m), 1460(m), 1408(m), 1327(w), 1156(s), 1109(s), 1043(s), 920(s), 770(m), 594(s), 528(m), 472(m).

Synthesis of $[Ni_3(H_2L')_2(4,4'\text{-bipy})_2(H_2O)_2]{\cdot}4H_2O$ (2). A mixture of $Ni(Ac)_2{\cdot}4H_2O$ (0.25 g, 1 mmol), H_5L' (0.13 g, 0.5 mmol) and 4,4'-bipy (0.09 g, 0.5 mmol) was dissolved in 10 mL distilled water , and then stirred for about 1 hour at room temperature. The mixture (pH = 6.0) was sealed in a 20 mL Teflon–lined stainless steel autoclave, and heated at 180 °C for 5 days under autogenous pressure. After the mixture was cooled slowly to room temperature, the green block crystals of **2**

were obtained. Yield 39.1% (based on Ni). Anal. Calc. for $C_{28}H_{44}N_6O_{22}P_4Ni_3$: C, 30.12; H, 3.97; N, 7.53; P, 11.10; Ni, 15.76. Found: C, 30.16; H, 3.93; N, 7.56; P, 11.15; Ni, 15.71 %. IR (KBr, cm^{-1}): 3434(m), 3053(w), 2921(m), 2855(w), 1610(s), 1532(m), 1496(w), 1423(m), 1330(w), 1152(s), 1120(s), 1025(m), 917(m), 863(w), 770(m), 594(m), 540(m), 461(w).

Crystallographic studies

Data collections for compounds **1** and **2** were performed on the Bruker AXS Smart APEX II CCD X–diffractometer equipped with graphite monochromated Mo$K\alpha$ radiation (λ = 0.71073 Å) at 293 ± 2K. An empirical absorption correction was applied by using the SADABS program. All structures were solved by direct methods and refined by full–matrix least squares fitting on F^2 by SHELXS–97.[10] All non–hydrogen atoms were refined anisotropically. Hydrogen atoms of organic ligands were generated geometrically with fixed isotropic thermal parameters, and included in the structure factor calculations. Hydrogen atoms for water molecules were not included in the refinement. Details of crystallographic data and structural refinements of compounds **1** and **2** are summarized in Table 1. Selected bond lengths are given in Table 2. Selected bond angles are listed in Table S1.

Table 1

Table 2

Results and discussion

Syntheses

Two new nickel(II) carboxyphosphonates with a 3D pillared-layered structure have been synthesized under hydrothermal conditions. With the aim to explore optimum method for obtaining pure phase materials, two systematical experimental investigations have been designed. The first experiment was designed to investigate the influence of the anions of nickel salts on the reaction products. Thus, four different nickel salts $NiCl_2·6H_2O$, $Ni(Ac)_2·4H_2O$, $Ni(NO_3)_2·6H_2O$ and $NiSO_4·6H_2O$ were reacted keeping a constant Ni(II)/4,4'-bipy/H_5L = 1:0.5:0.5 ratio at their original pH (T = 170 °C, 120 h). Our experiment demonstrates that the final reaction products synthesizing by different nickel salts exhibit different phases. $Ni(Ac)_2·4H_2O$ (original pH = 6), $Ni(NO_3)_2·6H_2O$

(original pH = 5) and $NiSO_4 \cdot 6H_2O$ (original pH = 5) acting as reactants synthesize amorphous powders. However, the pure phase (green crystals) for compound **1** are obtained by $NiCl_2 \cdot 6H_2O$ (original pH = 6). So we realize that $NiCl_2 \cdot 6H_2O$ may be more adaptable nickel salts as the reactant to synthesize compound **1**. One other variable that has a profound impact on the product formation is the pH value. The system using $NiCl_2 \cdot 6H_2O$ as nickel salts at different pH was studied. Unexpectedly, the pure phase of large block single crystals for compound **1** is obtained when at original pH of 6 without adding NaOH or HCl. However, the formation of amorphous powders, mixture phases or green clear solution for compound **1** comes into being at other pH value. The results of two experimental investigations show that $NiCl_2 \cdot 6H_2O$ is regard as the optimal nickel salt to synthesize compound **1** at original pH = 6 keeping a constant Ni(II)/4,4'-bipy/H_5L = 1:0.5:0.5 ratio (T = 170 °C, 120 h). The analogous experimental investigations were also designed to obtain the optimum method for synthesizing compound **2**. The powder XRD patterns and the simulated XRD patterns of the two title compounds are shown in ESI (Fig. S1, Fig. S2).

Description of the crystal structures

X-ray single crystal diffraction revealed that compound **1** crystallizes in the monoclinic space group *C*2/c (see Table 1). As shown in Fig. 1, the asymmetric unit of compound **1** contains two crystallographically independent Ni(II) atoms (occupancy: Ni(1) 100%, Ni(2) 50%), one H_2L^{3-} anion, half a 4,4'-bipy and two coordinated water molecules. Ni(1) exhibits six-coordinated environment. Five of the six coordination positions are filled with N1 atom and four phosphonate oxygen atoms (O1, O4, O3B and O6C) from three separate H_2L^{3-} anions, and the remaining site is occupied by N2 atom from the coordinated 4,4'-bipy ligand. Ni(2) is octahedrally coordinated to two phosphonate oxygen atoms (O2 and O2D) from two separate H_2L^{3-} anions and four oxygen atoms (O9, O9D, O10 and O10D) from four coordinated water molecules. The Ni–O bond lengths fall between 2.026(3) and 2.103(3) Å, and the Ni–N bond lengths are 2.083(4) and 2.262(3) Å (Table 2). These values are in agreement with those reported for other Ni(II) phosphonates.[11] The H_2L^{3-} acts as a hexadentate bridging mode and links with four Ni(II) atoms through N1 and five phosphonate oxygen atoms (O1, O2, O3, O4 and O6). The carboxylate oxygen atoms (O7, O8) are not involved in the coordination of Ni(II) atoms. The phosphonate oxygen atoms (O1, O2, O3, O4 and O6) are all monodentaten (Fig. 2a). Based on the charge balance, the phosphonate oxygen atom (O5) and carboxylate oxygen atom (O7) are protonated.

Fig. 1

Fig. 2

Compound **1** exhibits a three-dimensional framework with pillared-layered structure (Fig. 4). As shown in Fig. 3a, each {Ni(1)O_4N_2} octahedron connects four {CPO_3} tetrahedra through four phosphonate oxygen atoms and {Ni(2)O_6} octahedron links two {CPO_3} tetrahedra through two phosphonate oxygen atoms. The {Ni(1)O_4N_2}, {Ni(2)O_6} and {CPO_3} polyhedra are interconnected *via* corner-sharing into a 2D inorganic player in the *bc*-plane. The result of connections in this manner is formation of regular windows made up of 16 atoms, which consist of four Ni, four P and eight O atoms with the sequences Ni1–O6–P2–O4–Ni1–O6–P2–O4–Ni1–O1–P1–O2–Ni2–O2–P1–O3 in the inorganic layer (Fig. 3b). Then adjacent 2D inorganic layers are further cross-linked *via* 4,4′-bipy ligands to form a 3D pillar-layered structure, which contains channels with a size of about 9 × 11 Å based on the crystal structure. The benzoic acid moieties are located in these channels.

Fig. 3

Fig. 4

Compound **2** crystallizes in the monoclinic space group *C*2/c (see Table 1). As shown in Fig. 5, the asymmetric unit of the structure for compound **2** is comprised of two Ni(II) atoms (occupancy: Ni(1) 100%, Ni(2) 50%), one $H_2L'^{3-}$ anion, two half-occupied 4,4'-bipy moieties and two coordinated water molecules (occupancy: O9 50%, O10 50%). Ni(1) is located in an octahedral environment by three phosphonate oxygen atoms (O1A, O3 and O4) and one carboxylate oxygen atom (O7) from two separate $H_2L'^{3-}$ anions, as well as two nitrogen atoms (N1 and N2) from a $H_2L'^{3-}$ anion and a 4,4'-bipy ligand. Ni(2) is six-coordinated by two carboxylate oxygen atoms (O8 and O8A) from two separate $H_2L'^{3-}$ anions, two nitrogen atoms (N3 and N3B) from two 4,4'-bipy

ligands, and two oxygen atoms (O9 and O10) from two coordinated water molecules. The Ni–O distances are in the range of 2.0209(15) to 2.121(5) Å and the Ni–N bond lengths are in the range from 2.0825(15) to 2.1315(15) Å (Table 2). These distances are comparable to those reported for other Ni(II) phosphonates.[11] The $H_2L'^{3-}$ can be described as a hexadentate bridging mode, binding three Ni(II) atoms through one nitrogen atom (N1), three phosphonate oxygen atom (O1, O3, O4) and two carboxylate oxygen atoms (O7, O8). The oxygen atoms (O1, O3, O4, O7 and O8) are all monodentate (Fig. 2b). The phosphonate oxygen atoms (O2, O6) are protonated based on P–O distances and charge balance.

Fig. 5

Fig. 6

Fig. 7

Compound **2** also features a 3D pillar-layered architecture (Fig. 7b). The interconnection of Ni(1) atoms by chelating and bridging $H_2L'^{3-}$ anions results in a 1D helical chain of $\{Ni(1)(H_2L')\}^-$ along the *b*-axis (Fig. 6c). Adjacent so-built chains are bridged by $\{Ni(2)O_4N_2\}$ octahedra to give rise to a 2D layer in the *ab*-plane (Fig. 6b). The connections in this manner lead to regular windows assembled with 32 atoms. In order to facilitate viewing, the window can be seen clearly in Fig. 6a, which is made up of eight Ni, four P, sixteen O and four C atoms with the sequences $(Ni1–O–P–O–Ni1–O–C–O–Ni2–O–C–O–Ni1–O–P–O)_2$ in the 2D layer. Such neighboring 2D layers are further cross-linked through 4,4'-bipy ligands, generating a 3D framework structure with a 1D channel system along the *b*-axis. The channel system running along the *b*-axis is formed by 42-membered rings composed of eight Ni(II) atoms, two 4,4'-bipy ligands, four carboxyl groups and two phosphonate groups of H_5L ligands (Fig. 7a). The size of the channel is estimated to be 11.1 Å (C11–C11) × 8.1 Å (C4–C4) based on structure data. The diameter of the pore (as shown by the green ball) inside the channel is estimated to be 8.1 Å (Fig. 7a). The lattice water molecules are located at the channel.

IR spectroscopy

The IR spectra for compounds **1** and **2** are recorded in the region 4000–400 cm^{-1} (Fig. S3, Fig. S4, ESI). The absorption band at 3582 cm^{-1} and 3523 cm^{-1} for **1** can be assigned to the O–H stretching vibrations of water molecules and hydroxyl groups, and the absorption band at 3434 cm^{-1} for **2** is due to the O–H stretching vibrations of water molecules. The C–H stretching vibrations are observed as sharp, weak bands close to 3000 cm^{-1} for compounds **1** and **2**. The asymmetric and symmetric vibrations of the carboxylate group centered at 1702 and 1460 cm^{-1} for **1** are observed, which are the expectative value of uncoordinated carboxylic acids.[12] The fairly broad bands at 1612 and 1423 cm^{-1} for **2** is assigned to the C=O asymmetric and symmetric stretching vibrations of the carboxylic acid group. Its rather low position is typical for constellations where both oxygen atoms of the COOH group coordinated to the metal.[13] The bands at 1610, 1540 and 1408 cm^{-1} for **1**, as well as at 1532, 1496 and 1330 cm^{-1} for **2**, can be assigned to the stretching bands of the pyridyl rings of 4,4'-bipy ligands.[14] Strong bands between 1200 and 900 cm^{-1} for two compounds are due to stretching vibrations of the tetrahedral CPO_3 groups, as expected.[15] Additional medium and weak bands at low energy for **1** and **2** are found, which are likely assigned to bending vibrations of the tetrahedral CPO_3 groups.

Thermal analyses

Thermogravimetric analysis diagram of compounds **1** and **2** have been performed in the temperature range of 50–1100 °C in static air atmosphere (Fig. S5, Fig. S6, ESI). Compound **1** was thermally stable up to 158 °C. Above this temperature, the TG curve shows three steps of weight losses for compound **1**. At approximately 192 °C, compound **1** completes its first step of weight loss, corresponding to the release of four coordinated water molecules. The weight loss of 6.7% is consistent with the calculated value (7.0%). A second weight loss occurs between 308 and 638 °C, which can be attributed to the combustion of 4,4′-bipy ligands and partial decomposition of carboxyphosphonate ligands. The third stage occurring between 726 and 980 °C corresponds to the further decomposition of the compound. The final product is $Ni_2P_2O_7$ based on XRD power diffraction (Fig. S7, ESI). The total weight loss at 980 °C is 53.0%. Compound **2** also indicates three complicated overlapping steps of weight losses. The first step stated at 50 °C and was completed at 204 °C, corresponding to the loss of four lattice water molecules and two coordinated water molecules. The observed weight loss of 9.7% is basically close to the calculated value

(10.4%). The second weight loss occurs at 307−519 °C, which can be attributed to the pyrolysis of 4,4′-bipy ligands and partial decomposition of organic moieties. The last weight loss started at 814 °C and ended at 972 °C, corresponding to the further decomposition of the compound. The final residue has a powder diffraction pattern, corresponding to $Ni_2P_2O_7$ (Fig. S8, ESI). The total weight loss at 972 °C is 70.9%.

Surface photovoltage properties

The contactless and nondestructive technique of surface photovoltage spectroscopy (SPS) can be used to investigate the photophysics of the excited states and the surface charge behavior of the sample. This technique not only relates to the electron transitions under light-inducement, but also reflects the separation and transfer of photo-generated charges as well as optical absorption characteristics of semiconductor samples.[16] Surface photovoltage spectroscopy (SPS) of compounds **1** and **2** was measured with a solid junction photovoltaic cell (ITO/sample/ITO) in the range of 300–800 nm. The detected SPS signal is equivalent to the change in the surface potential barrier on illumination (δV_s), which is given by the equation: $\delta V_s = V_s' - V_s^o$, where V_s' and V_s^o are the surface potential barriers before and after illumination, respectively. As far as band to band transitions are concerned, a positive response of surface photovoltage (SPV) ($\delta V_s > 0$) means that the sample is characterized as a *p*-type semiconductor, whereas a negative response is an *n*-type semiconductor.[17]

Fig. 8

Table 3

The SPS of compounds **1** and **2** are shown in Fig. 8a and Fig. 8b, respectively. They all appear as SPV response bands between 300 and 800 nm. It can be seen that the signal detected by SPS at 300–600 nm is a wide peak. The signal is actually the results of overlap of several response bands. To make the assignment of each response band clear, we separated them by the Origin 7.0 program. As shown in Fig. 8a, compound **1** contains three filial bands at 368 nm, 457 nm and 507 nm. The response band at λ_{max} = 368 nm can be attributed to the LMCT transition (from ligand to metal charge transfer transition) while the response bands at λ_{max} = 457 nm and 507 nm are assigned to the

d→d* transitions of Ni(II) ions. The SPS of compound **2** is similar to that of compound **1**. After Origin 7.0 treatment, three response bands at 376 nm, 452 nm and 501 nm are observed (Fig. 8b). The former response band at $\lambda_{max} = 376$ nm may be assigned to the LMCT transition (from ligand to metal charge transfer transition) and the latter two response bands are attributed to the d→d* transitions of Ni(II) ions (see Table 3). Compounds **1** and **2** all present three SPV responses in the range of 300–800 nm, which indicates that they possess semiconductor characteristics. Upon comparing the SPV responses of compound **1** and compound **2**, it can be seen that without the external electric field the values of the two compounds' response bands are similar, which can be attributed to the coordination environment of Ni(II) ions in compounds **1** and **2**. They both have two species of coordinated atoms (N and O), the band-to-band transitions caused by LMCT (ligand-to-metal charge transfer) appear two species (O→Ni and N→Ni).[8] Whereas the intensities of their SPV responses are obviously different, which may be due to the differences in their structures.[5a] Compounds **1** and **2** both possess 3D structures (Fig. 4 and Fig. 7b), whereas compound **1** contains $\{Ni(1)O_4N_2\}$ and $\{Ni(2)O_6\}$ octahedra, compound **2** only contains $\{NiO_4N_2\}$ octahedron. Furthermore, the carboxylate oxygen atoms of carboxyphosphonate ligands are coordinated to Ni(II) ions in compound **2** but not in compound **1**. When we compared the SPV responses of the two title compounds with other coordination polymer materials, the different intensities have been seen. The SPV response intensity of compounds **1** and **2** is higher than that of $[FeCd_2(Hcit)_2(H_2O)_2]_n$ and $[Ni(opha)(Phen)(H_2O)_3]\cdot H_2O$.[18] In our recent work, a few investigations on the surface photovoltage property of metal phosphonates have been reported, in which surface photovoltage properties have been observed in some Mn(II), Fe(II), Co(II), Ni(II) and Cu(II) phosphonates.[8] Results from ours and other groups indicate that not only semiconductor possess photovoltage characteristic, some coordination polymer materials with the semiconductor characteristic also can exhibit the photovoltage property. Therefore, compounds **1** and **2** can be regarded as potential semiconductor materials.

Field-induced surface photovoltage spectroscopy (FISPS) can be measured by applying an external electric field to the sample with a transparent electrode. For a *p*-type semiconductor, when a positive electric field is applied on the semiconductor surface, the SPV response increases since the external field is consistent with the built-in field. On the contrary, when a negative electric field is applied, the SPV response is weakened. In contrast to *p*-type semiconductors, the SPV response intensity of *n*-type semiconductors increases as a negative field is applied and reduces as a positive

electric field is applied. Fig.8 also shows the FISPS of the two compounds in the range of 300–800 nm when the external electric fields are –0.5, 0 and +0.5 V, respectively. The SPV response intensities of compound **1** increase when the positive fields increase, while they reduce when the external negative fields increase **(**Fig. 8c). This is attributed to the positive electric field being beneficial to the separation of photoexcited electron–hole pairs, which in turn results in an increase of response intensity; however, the negative electric field has just the opposite effect. The FISPS confirms the *p*-type characteristic of compound **1**. The SPV response intensities of compound **2** reduce when the positive fields increase, while they increase when the external negative fields increase (Fig. 8d). This is attributed to the negative electric field being beneficial to the separation of photoexcited electron–hole pairs, which in turn results in a reduce of response intensity; however, the positive electric field has just the opposite effect. The FISPS confirms the *n*-type characteristic of compound **2**.

Fig. 9

Luminescent properties

The solid-state emission spectra of 4,4′-bipy ligand, free H_5L ligand (Fig. S9, Fig. S10, ESI) and compounds **1** and **2** (Fig. 9) were measured at room temperature. The 4,4′-bipy ligand shows a fluorescent emission band at 418 nm upon excitation at 348 nm and the free carboxyphosphonate ligand H_5L displays fluorescent emission bands at 337 and 349 nm upon excitation at 308 nm, whereas the free H_5L' ligand shows no emission in the visible region.[19] In contrast, compounds **1** and **2** give relatively strong fluorescent emissions under the same experimental conditions. The two compounds both display a purple fluorescent emission band at λ_{max} = 419 nm (Fig. 9) upon the same excitation at 370 nm. The emission spectra of compounds **1** and **2** are very similar to that of discrete 4,4′-bipy ligand, and it demonstrates that the emission spectra of compounds **1** and **2** are neither metal-to-ligand charge transfer (MLCT) nor ligand-to-metal charge transfer (LMCT) in nature but rather are attributed to an intraligand emission state.[20] Compared to the free 4,4′-bipy ligand, the fluorescent spectra of compounds **1** and **2** are slightly enhanced in intensity in the emission band, which can be attributed to the fact that 4,4′-bipy ligands coordinated to Ni(II) ions

would impose rigidity.[21] Unfortunately, the luminescent lifetimes of compounds **1** and **2** are not observed, since the lifetimes of compounds **1** and **2** are too short to be measured. The difference in the relative intensities of the peaks in the emission spectra of compounds **1** and **2** is probably due to the introduction of different carboxyphosphonate ligands.[5c] Therefore, luminescence mechanisms of compounds **1** and **2** should be assigned to the intraligand emission state and the luminescence behavior is closely associated with the ligands coordinated around the center Ni(II) ions.[22] The investigation of luminescent properties indicates that compounds **1** and **2** are good candidates for purple-light luminescent materials.

Conclusions

In summary, two new nickel(II) carboxyphosphonates with a 3D pillar-layered structure, namely, $[Ni_3(H_2L)_2(4,4'\text{-bipy})(H_2O)_4]$ **(1)** and $[Ni_3(H_2L')_2(4,4'\text{-bipy})_2(H_2O)_2]\cdot 4H_2O$ **(2)** have been synthesized by hydrothermal technique, using H_5L or H_5L' as the phosphonate ligand and 4,4′-bipy as the second metal linker. Compounds **1** and **2** both feature three-dimensional (3D) framework structures with two-dimensional (2D) layers pillared by 4, 4′-bipy. For compound **1**, $\{Ni(1)O_4N_2\}$, $\{Ni(2)O_6\}$ and $\{CPO_3\}$ polyhedra form a 2D inorganic layer in the *bc*-plane by the mode of corner-sharing. Neighboring layers are further supported by 4,4′-bipy ligands to form a 3D pillar-layered structure. In compound **2**, $\{Ni(1)O_4N_2\}$, $\{Ni(2)O_4N_2\}$ and $\{CPO_3\}$ polyhedra are interconnected by carboxyphosphonate ligands to a 2D layer in the *ab*-plane, which are further cross-linked into a 3D framework structure *via* 4,4'-bipy ligands. We have systematically investigated the influence of different metal salts and pH value on the synthesis of two title compounds. The SPS and FISPS of compounds **1** and **2** indicate that they possess SPV responses in the range of 300–800 nm and show p-type and n-type semiconductor characteristics, respectively. The luminescence analyses indicate that compounds **1** and **2** may be candidates for potential luminescent materials. Furthermore, the 4,4′-bipy as a second organic ligand also plays a very important role in the two compounds' structures and properties.

Acknowledgments

This work is supported by the National Natural Science Foundation of China (Grant No. 21371085).

Electronic supplementary information (ESI) available: X-ray crystallographic files in CIF format for compounds **1**and **2**. IR spectra of compounds **1** and **2**, XRD pattern of the final products in the thermal decomposition for compounds **1**and **2** as well as XRD patterns of the experiments compared to those simulated from X-ray single-crystal data for compounds **1** and **2**. CCDC 1011162 (**1**) and 1011163 (**2**) contain the supplementary crystallographic data for this paper. These data can be obtained free of charge www.ccdc.cam.ac.uk/conts/retrieving.html (or from the Cambridge Crystallographic Data Center, 12, Union Road, Cambridge CB21EZ, UK; fax: (+44) 1223–336–033; e–mail: deposit@ccdc.cam.ac.uk).

References

1. (a) M. Bazaga-García, R. M. P. Colodrero, K. D. Demadis, *J. Am. Chem. Soc.*, 2014, **136**, 5731; (b) A. Clearfield and K. Demadis, *Metal Phosphonate Chemistry: From Synthesis to Applications*, Royal Society of Chemistry, Oxford, 2012, p. 164; (c) H. Hirao and K. Morokuma, *J. Am. Chem. Soc.,* 2010, **132**, 17901; (d) P. O. Adelani and T. E. Albrecht-Schmitt, *Inorg. Chem.,* 2010, **49**, 5701; (e) M. Plabst, L. B. McCusker and T. Bein, *J. Am. Chem. Soc.,* 2009, **131**, 18112; (f) W. Ouellette, M. H. Yu, C. J. O'Connor and J. Zubieta, *Inorg. Chem.,* 2006, **45**, 7628.
2. (a) R. B. Fu, S. M. Hu and X. T. Wu, *CrystEngComm*., 2013, **15**, 802; (b) J. Weber, G. Grossmann, K. D. Demadis, N. Daskalakis, E. Brendler, M. Mangstl and J. S. Auf der. Günne, *Inorg. Chem.,* 2012, **51**, 11466; (c) P. O. Adelani and T. E. Albrecht-Schmitt, *Cryst. Growth Des.,* 2011, **11**, 4676; (d) S. F. Tang, X. B. Pan, X. X. Lv, S. H. Yan, X. R. Xu, L. J. Li and X. B. Zhao, *CrystEngComm*., 2013, **15**, 1860.
3. (a) S. P. Shi, Y. Y. Zhu, Z. G. Sun, W. Zhou, L. L. Dai, M. X. Ma, W. Z. Li, H. Luo and T. Sun, *Cryst. Growth Des.*, 2014, **14**, 1580; (b) W. Chu, Z. G. Sun, C. Q. Jiao, Y. Y. Zhu, S. H. Sun, H. Tian and M. J. Zheng, *Dalton Trans*., 2013, **42**, 8009; (c) F. Tong, Z. G. Sun, K. Chen, Y. Y. Zhu, W. N. Wang, C. Q. Jiao, C. L. Wang and C. Li, *Dalton Trans.,* 2011, **40**, 5059; (d) Y. Y. Zhu, Z. G. Sun, Y. Zhao, J. Zhang, X. Lu, N. Zhang, L. Liu and F. Tong, *New J. Chem.,* 2009, **33**, 119.
4. (a) H. Zhu, J. Huang, S. S. Bao, M. R. and L. M. Zheng, *Dalton Trans.*, 2013, **42**, 14075.; (b) H. Y. Wu, W. T. Yang and Z. M. Sun, *Cryst. Growth Des.*, 2012, **12**, 4669; (c) Z. Y. Du, H. B. Xu,

X. L. Li and J. G. Mao, *Eur. J. Inorg. Chem.*, 2007, 4520.

5. (a) S. H. Sun, Z. G. Sun, Y. Y. Zhu, D. P. Dong, C. Q. Jiao, J. Zhu, J. Li, W. Chu, H. Tian, M. J. Zheng, W. Y. Shao and Y. F. Lu, *Cryst. Growth Des.*, 2013, **13**, 226; (b) M. J. Zheng, Y. Y. Zhu, Z. G. Sun, J. Zhu, C. Q. Jiao, W. Chu, S. H. Sun and H. Tian, *CrystEngComm.*, 2013, **15**, 1445; (c) L. L. Dai, Y. Y. Zhu, C. Q. Jiao, Z. G. Sun, S. P. Shi, W. Zhou, W. Z. Li, T. Sun, H. Luo and M. X. Ma, *CrystEngComm.*, 2014, **16**, 5050; (d) K. Chen, Z. G. Sun, Y. Y. Zhu, Z. M. Liu, F. Tong, D. P. Dong, J. Li, C. Q. Jiao, C. Li and C. L. Wang, *Cryst. Growth. Des.,* 2011, **11**, 4623; (e) C. Q. Jiao, J. C. Zhang, Y. Zhao, Z. G. Sun, Y. Y. Zhu , L. L. Dai, S. P. Shi and W. Zhou, *Dalton Trans.*, 2014, **43**, 1542.
6. L. Kronik and Y. Shapira, *Surface Science Reports*, 1999, **37**, 85.
7. (a) D. J. Wang, J. Zhang, T. S. Shi, B. H. Wang, X. Z. Cao and T. J. Li, *J. Photochem. Photobiol., A,* 1996, **93**, 21; (b) U. Weiler, T. Mayer, W. Jaegermann, C. Kelting, D. Schlettwein, S. Makarov and D. Wöhrle, *J. Phys. Chem. B,* 2004, **108**, 19398; (c) T. Uekermann, D. Schlettwein and N. I. Jaeger, *J. Phys. Chem. B*, 2001, **105**, 9524; (d) L. Zhang, S. Y. Niu, J. Jin, L. P. Sun, G. D. Yang and L. Ye, *Inorg. Chim. Acta*, 2009, **362**, 1448.
8. (a) D. P. Dong, Z. G. Sun, F. Tong, Y. Y. Zhu, K. Chen, C. Q. Jiao, C. L. Wang, C. Li and W. N. Wang, *CrystEngComm*., 2011, **13**, 3317; (b) C. Li, C. Q. Jiao, Z. G. Sun, K. Chen, C. L. Wang, Y. Y. Zhu, J. Zhu, Y. Zhao, M. J. Zheng, S. H. Sun, W. Chu and H. Tian, *CrystEngComm*., 2012, **14**, 5479; (c) H. Tian, Y. Y. Zhu, Z. G. Sun, F. Tong, J. Zhu, W. Chu, S. H. Sun and M. J. Zheng, *New J. Chem*., 2013, **37**, 212; (d) W. Zhou, Y. Y. Zhu, C. Q. Jiao, Z. G. Sun, S. P. Shi, L. L. Dai, T. Sun, W. Z. Li, M. X. Ma and H. Luo, *CrystEngComm.*, 2014, **16**,1174.
9. (a) S. Bauer, T. Bein and N. Stock, *Inorg. Chem.*, 2005, **44**, 5882; (b) J. G. Mao, Z. Wang and A. Clearfield, *New J. Chem*., 2002, **26**, 1010.
10. G. M. Sheldrick, *Acta Crystallogr., Sect. A: Found. Crystallogr.*, 2008, **64**, 112.
11. (a) K. R. Ma, J. N. Xu, L. R. Zhang, J. Shi, D. J. Zhang, Y. L. Zhu, Y. Fan and T. Y Song, *New J. Chem.*, 2009, **33**, 886; (b) D. Y. Kong, D. G. Medvedev, and A. Clearfield, *Inorg. Chem.*, 2004, **43**, 7308; (c) X. J. Li, Y. Z Cai, Z. L Fang, L. J. Wu, B. Wei and S. Lin, *Cryst. Growth Des.*, 2011, **11**, 4517.
12. N. Stock and T. Bein, *J. Mater. Chem.*, 2005, **15**, 1384.
13. A. Cabeza, M. A. G. Aranda and S. Bruque, *J. Mater. Chem.,* 1998, **8**, 2479.

14. (a) N. G. Armatas, W. Ouellette, K. Whitenack, J. Pelcher, H. X. Liu, E. Romaine, C. J. O'Connor and J. Zubieta, *Inorg. Chem.*, 2009, **48**, 8897; (b) R. T. Clarke, K. Latham, C. J. Rix and M. Hobday, *Chem. Mater.*, 2004, **16**, 2463.
15. (a) A. Cabeza, X. Ouyang, C. V. K. Sharma, M. A. G. Aranda, S. Bruque and A. Clearfield, *Inorg. Chem*., 2002, **41**, 2325; (b) Z. M. Sun, J. G. Mao, B. P. Yang and S. M. Ying, *Solid State Sci*., 2004, **6**, 295.
16. (a) Y. H. Lin, D. J. Wang, Q. D. Zhao, M. Yang and Q. L. Zhang, *J. Phys. Chem. B*, 2004, **108**, 3202; (b) B. F. Xin, L. Q. Jing, Z. Y. Ren, B. Q. Wang and H. G. Fu, *J. Phys. Chem. B*, 2005, **109**, 2805; (c) L. Q. Jing, X. J. Sun, J. Shang, W. M. Cai, Z. L. Xu, Y. G. Du and H. G. Fu, *Sol. Energy Mater. Sol. Cells*, 2003, **97**, 133; (d) J. Zhang, D. J. Wang, Y. M. Chen, T. J. Li, H. F. Mao, H. J. Tian, Q. F. Zhou and H. J. Xu, *Thin Solid Films*, 1997, **300**, 208.
17. (a) S. Z. Li, J. W. Zhao, P. T. Ma, J. Du, J. Y. Niu, J. P. Wang, *Inorg. Chem.,* 2009, **48**, 9819; (b) Q. X. Han, P. T. Ma, J. W. Zhao, Z. L. Wang, W. H. Yang, P. H. Guo, J. P. Wang, J. Y. Niu, *Cryst. Growth Des.*, 2011, **11**, 436. (c) L. Li, S. Y. Niu, D. Li, J. Jin, Y. X. Chi, Y. H. Xing, *Inorg. Chem. Commun.*, 2011, **14**, 993.
18. (a) L. Li, J. Jin, Z. F. Shi, *Inorg. Chim. Acta*, 2010, 363, 748; (b) L. P. Sun, S. Y. Niu, J. Jin, *Inorg. Chem. Commun.*, 2006, **9**, 679.
19. J. L. Song, H. H. Zhao, J. G. Mao and K. R. Dunbar, *Chem. Mater.*, 2004, **16**, 1884.
20. (a) Y. Gong, W. Tang, W. B. Hou, Z. Y. Zha and C. W. Hu, *Inorg. Chem.,* 2006, **45**, 4987; (b) M. S. Wang, G. C. Guo, M. L. Fu, L. Xu, L. Z. Cai and J. S. Huang, *Dalton Trans.,* 2005, 2899; (c) W. Chen, J. Y. Wang, C. Chen, Q. Yue, H. M. Yuan, J. S. Chen and S. N. Wang, *Inorg. Chem.,* 2003, **42**, 944.
21. T. Ma, M. X. Li, Z. X. Wang, J. C. Zhang, *Cryst. Growth Des.*, 2014, **14**, 4155.
22. Q. P. Li and J. J. Qian, *RSC Adv.*, 2014, **4**, 32391.

Table 1 Crystal data and structure refinements for compounds **1** and **2**

Compounds	**1**	**2**
Formula	$C_{30}H_{40}N_4O_{20}P_4Ni_3$	$C_{28}H_{44}N_6O_{22}P_4Ni_3$
Fw	1076.61	1116.70
Crystal system	Monoclinic	Monoclinic
Space group	*C*2/c	*C*2/c
A (Å)	25.769(2)	27.790(3)
B (Å)	9.7059(9)	8.1036(7)
C (Å)	17.2986(16)	22.617(2)
β (°)	104.016(2)	123.1290(10)
V (Å$^{3)}$	4197.7(7)	4265.4(7)
Z	4	4
D_{cacl} (g·cm^{-3})	1.704	1.739
μ (mm^{-1})	1.567	1.550
F(000)	2208	2296
T (K)	295(2)	295(2)
Theta range (°)	1.63 to 26.49	1.75 to 26.49
Reflections collected/unique	11590, 4338 (R_{int} = 0.0436)	11747, 4392 (R_{int} = 0.0268)
GOF on F^2	1.058	1.044
R_1, wR_2 [a] [I>2σ (I)]	0.0494, 0.1237	0.0640, 0.1945
R_1, wR_2 [a] (all data)	0.0701, 0.1344	0.0764, 0.2091
$(\Delta\rho)_{Max}$, $(\Delta\rho)_{min}$/e Å^{-3}	1.140, –0.647	4.237 , –0.987

[a] $R_1 = \Sigma\,(|F_0|-|F_C|) / \Sigma\,|F_0|$, $wR_2 = [\Sigma\, w\,(|F_0|-|F_C|)^2 / \Sigma\, w\, F_0^2]^{1/2}$.

Table 2 Selected bond lengths (Å) for compounds **1** and **2**.

Compound **1**			
Ni(1)–O(4)	2.026(3)	Ni(2)–O(2)	2.049(3)
Ni(1)–O(1)	2.059(3)	Ni(2)–O(2)#3	2.049(3)
Ni(1)–O(3)#1	2.062(3)	Ni(2)–O(9)#3	2.074(3)
Ni(1)–O(6)#2	2.066(3)	Ni(2)–O(9)	2.074(3)
Ni(1)–N(2)	2.083(4)	Ni(2)–O(10)#3	2.103(3)
Ni(1)–N(1)	2.262(3)	Ni(2)–O(10)	2.103(3)
Compound **2**			
Ni(1)–O(7)	2.0209(15)	Ni(2)–O(9)	2.0593(17)
Ni(1)–O(3)#1	2.032(5)	Ni(2)–O(8)	2.0659(13)
Ni(1)–N(2)	2.0825(15)	Ni(2)–O(8)#2	2.0659(13)
Ni(1)–O(1)	2.116(4)	Ni(2)–N(3)#2	2.0984(13)
Ni(1)–O(4)	2.121(5)	Ni(2)–N(3)	2.0984(13)
Ni(1)–N(1)	2.1315(15)	Ni(2)–O(10)	2.1174(17)

Symmetry transformations used to generate equivalent atoms:
#1 −x + 1/2, −y + 3/2, −z; #2 −x + 1/2, y – 1/2, −z + 1/2; #3 −x + 1/2, −y + 1/2, −z for **1**; #1 −x + 1/2, y + 1/2, −z + 1/2; #2 −x, y, −z + 1/2 for **2**.

Table 3 The SPV responses for compounds **1** and **2**

	λ_{max} (nm)	λ_{max} (nm)	λ_{max} (nm)
Compound 1	368	457	507
Compound 2	376	452	501
Assignment	LMCT	$d \rightarrow d^*$	$d \rightarrow d^*$

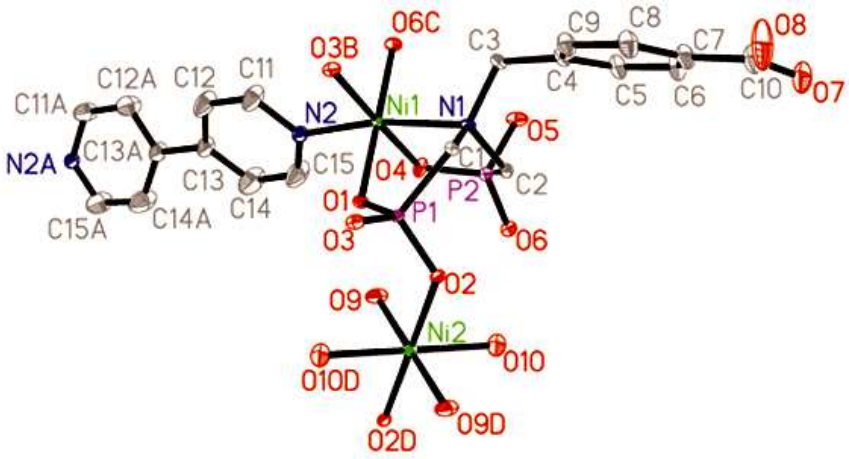

Fig. 1 Structure unit of compound **1** showing the atom labeling. Thermal ellipsoids are shown at the 50% probability level. All H atoms are omitted for clarity. Symmetry code for the generated atoms: (A) –x + 1/2, –y + 3/2, –z; (B) –x + 1/2, y + 1/2, –z + 1/2; (C) –x + 1/2, –y + 1/2, –z; (D) –x + 1/2, y – 1/2, –z + 1/2.

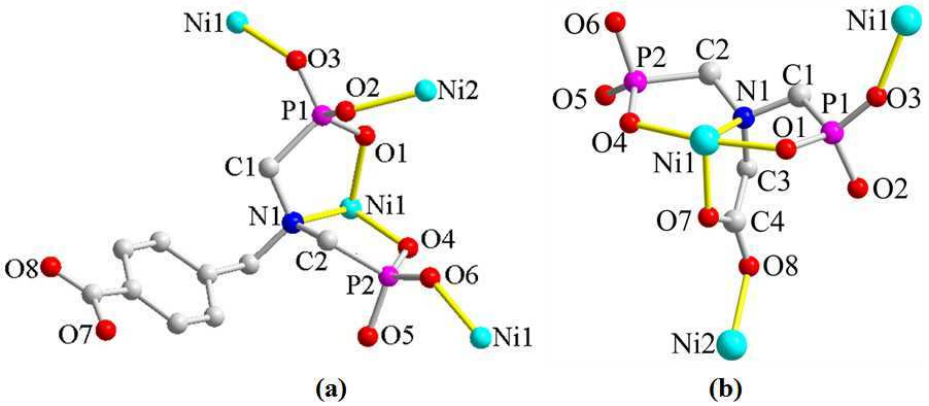

Fig. 2 (a) The coordination fashions of H_2L^{3-} in compound **1**; (b) the coordination fashions of $H_2L'^{3-}$ in compound **2**.

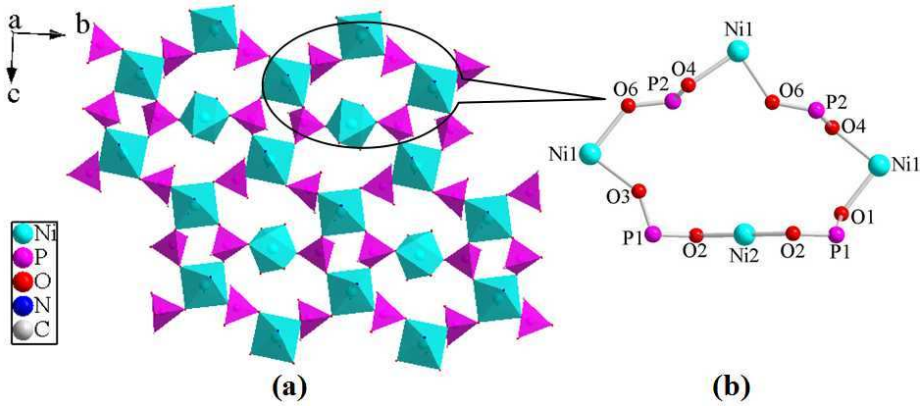

Fig. 3 (a) The 2D inorganic layer structure of compound **1** in the *bc*-plane; (b) the 16-atom rings in compound **1**.

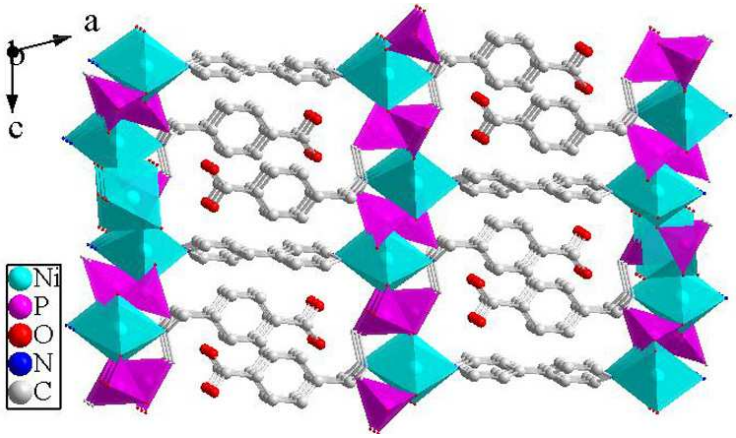

Fig. 4 View of the three-dimensional framework structure for compound **1** along the *b*-axis.

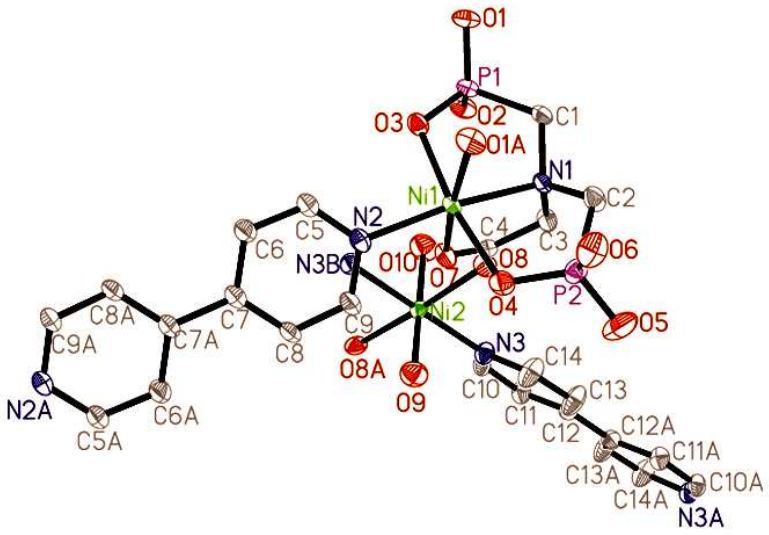

Fig. 5 Structure unit of compound **2** showing the atom labeling. Thermal ellipsoids are shown at the 50% probability level. All H atoms and lattice water molecules are omitted for clarity. Symmetry code for the generated atoms: (A) –x + 1/2, y – 1/2, –z + 1/2; (B) –x, y, –z + 1/2.

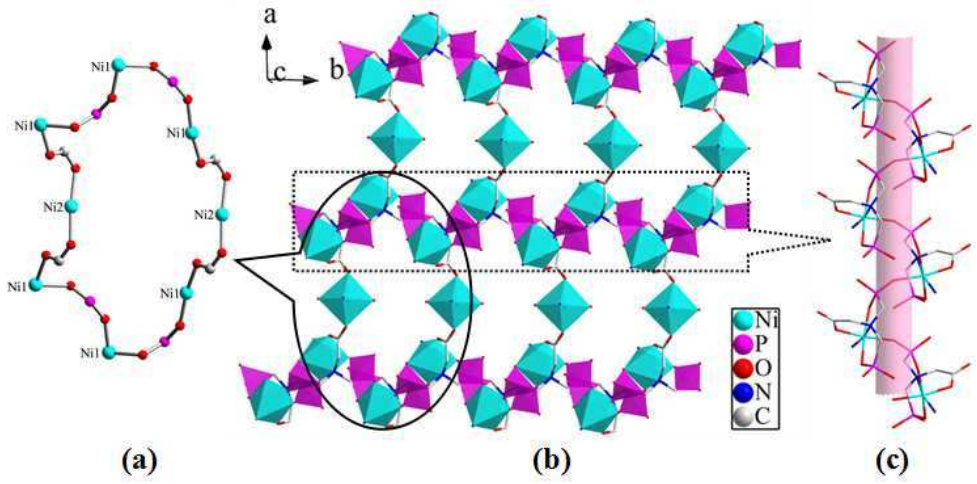

Fig. 6 (a) The 32-atom rings in compound **2**; (b) the 2D layer structure of compound **2** in the *ab*-plane; (c) the 1D chain structure of compound **2** along the *b*-axis.

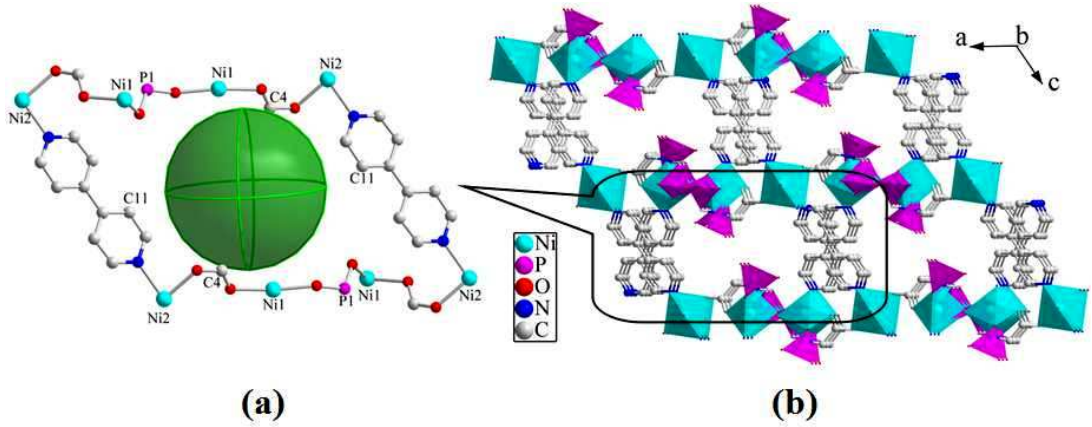

Fig. 7 (a) The 42-atom rings in compound **2**; the green sphere represents the pore defined within the frameworks, the diameter of the green ball inside the channels is 8.1 Å. (b) view of the three-dimensional framework for compound **2** along the *b*-axis.

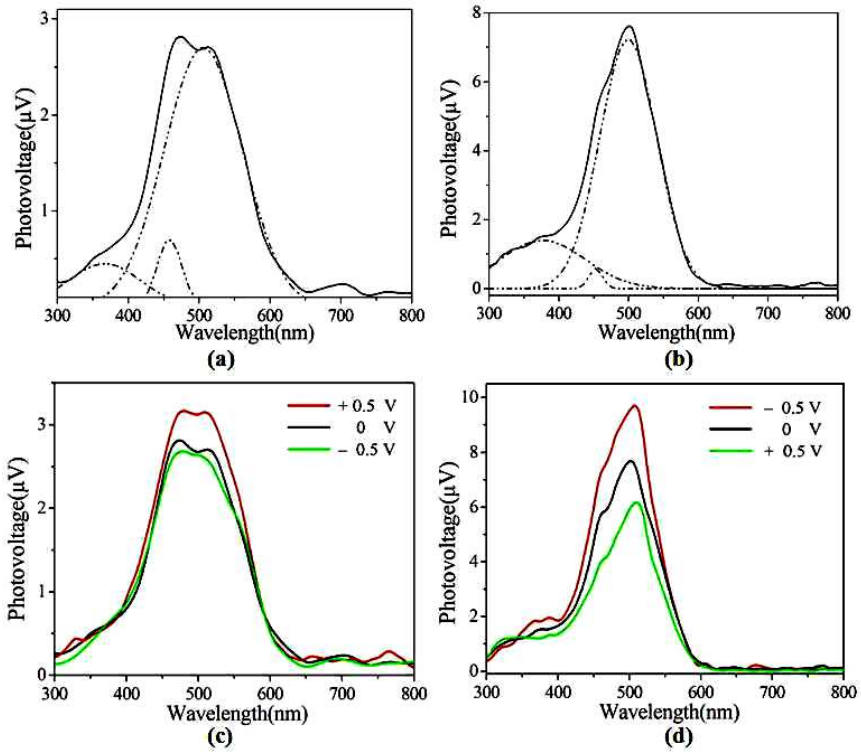

Fig. 8 (a) The SPS of compound **1**; **(b)** the SPS of compound **2; (c)** the FISPS of compound **1**; **(d)** the FISPS of compound **2**. The dotted lines are the SPV response bands obtained after treatment with Origin 7.0.

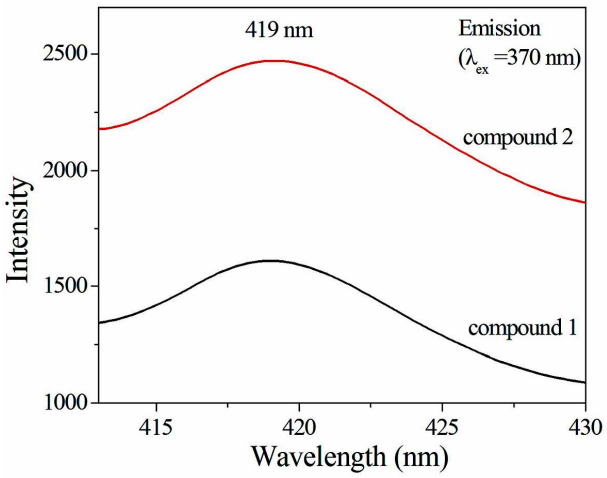

Fig. 9 Solid–state emission spectra of compounds **1** and **2** at room temperature.